CHEMISTRY
A EUROPEAN JOURNAL

DOI: 10.1002/chem.200900747

Lanthanide(III) Complexes with Two Hexapeptides Incorporating Unnatural Chelating Amino Acids: Secondary Structure and Stability

Federico Cisnetti, Christelle Gateau, Colette Lebrun, and Pascale Delangle*[a]

Abstract: Unnatural metal-chelating amino acids bearing aminodiacetate side-chains have been introduced into two hexapeptides to obtain efficient lanthanide-binding peptides. The synthesis of the enantiopure Fmoc-Ada$_n$-(tBu)$_2$-OH synthons is described with overall yields of 32 and 50% for $n=2$ and $n=3$ side-chain carbon atoms, respectively. The two peptides AcWAda$_n$PGAda$_n$GNH$_2$ (**P^n**) were synthesized from the protected synthons by standard solid-phase peptide synthesis. Studies of the lanthanide complexes of the two peptides **P^n** by luminescence titrations, mass spectrometry, circular dichroism, and solution NMR spectroscopy demonstrate that the Ada$_n$ chain length has a dramatic effect on the complexation properties. Indeed, the flexible compound **P^3** forms a mononuclear complex of moderate stability ($\beta_{11}=10^{9.9}$), which tends to transform into a binuclear species in the presence of excess of the metal ion. Interestingly, the more compact peptide **P^2** provides stable Ln^{3+} complexes with the exclusive formation of the mononuclear Ln**P^2** adduct. The stability constant of Tb**P^2** is two orders of magnitude higher ($\beta_{11}=10^{12.1}$) than that measured for **P^3**. The 800 MHz NMR spectrum of the La^{3+} complex of **P^2** evidences a well-defined type II β-turn as well as a hydrophobic Trp(indole)–Pro interaction. These interactions exemplify the non-innocent character of the peptide spacer in the complex La**P^2** as well as the role of a peptide secondary structure in the stabilization of metal complexes.

Keywords: amino acids · bioinorganic chemistry · lanthanides · peptides · structure elucidation

Introduction

Lanthanide trivalent ions (Ln^{3+}) are normally absent in living organisms. However, due to an ionic radius similar to that of the ubiquitous calcium ion (Ca^{2+}), Ln^{3+} cations can bind to proteins in Ca^{2+}-binding sites.[1] Common Ca^{2+}-binding loops in proteins such as calmodulin have 12 amino acids bearing side-chains with oxygen donors, such as acids or amides. In contrast to the absence of endogenous Ln^{3+} in biological media, Ln^{3+} chelates are gaining increasing importance in biological studies and biomedical applications due to their unique magnetic and photophysical properties. For instance, Gd^{3+} complexes are used as magnetic resonance imaging contrast agents,[2,3] other paramagnetic lanthanide cations as magnetic probes for structural NMR study in chemistry[4] and biology,[5] and emissive Tb^{3+} and Eu^{3+} complexes as optical probes with various applications in biology.[6] The introduction of Ln^{3+} ions into living organisms is a challenge for the coordination chemist because of their intrinsic toxicity. Ln^{3+} ions need to be encapsulated in ligands to form kinetically inert and/or thermodynamically stable complexes in vivo. Poly(aminocarboxylate) ligands have been extensively investigated because they carry a number of donor atoms close to or equal to the high coordination numbers (8 to 10) preferred by Ln^{3+}.[2] Complexation by such ligands avoids deleterious decoordination in vivo.

The use of peptides as Ln^{3+} ligands already adapted to the in vivo environment is an attractive idea. Small peptides derived from Ca^{2+}-binding proteins have been used as the starting point for the studies of Ln^{3+}–peptide complexes.[7] Ln^{3+} complexes of Ca^{2+}-binding EF-hand loops (as in calmodulin), designed by Franklin and co-workers to obtain artificial endonucleases and 33-mer peptides binding Ln^{3+} with micromolar affinities, have been investigated.[8] Imperiali and co-workers optimized the sequence of lanthanide-binding tags (LBTs) by using screening methods starting from Ca^{2+}-binding sites to obtain the highest possible affinity.[9,10]

[a] Dr. F. Cisnetti, Dr. C. Gateau, C. Lebrun, Dr. P. Delangle
INAC, Service de Chimie Inorganique et Biologique
(UMR E 3 CEA UJF, FRE CNRS 3200)
Commissariat à l'Energie Atomique
17 rue des martyrs, 38054 Grenoble Cedex (France)
Fax: (+33) 438785090
E-mail: pascale.delangle@cea.fr

Supporting information for this article is available on the WWW under http://dx.doi.org/10.1002/chem.200900747.

For instance, a 17-mer peptide has been demonstrated to bind Tb^{3+} in an eight-coordinate complex without any inner-sphere water molecules with a stability constant of $\log\beta_{11}^{pH7}=7.2$.[10] We recently reported a de novo designed cyclic decapeptide bearing four carboxyl side-chains, namely c(DREPGEWDPG). Although the solution structure of the apopeptide highlights a conformation suitable for complexing Ln^{3+} ions, with the four carboxyl side-chains oriented on the same face of the peptide scaffold, the stability of the lanthanide complexes is also in the micromolar range ($\log\beta_{11}^{pH7}\approx 6.5$).[11]

The above-mentioned examples show that there is an intrinsic limitation in the stability of lanthanide–peptide complexes if only natural amino acids are used. Indeed, the latter bear only simple binding groups, like carboxylates (Asp, Glu), phenolates (Tyr), or amides (Asn, Gln, backbone peptide linkage), which have a low affinity for Ln^{3+} in comparison with synthetic multidentate ligands of the poly(aminocarboxylate) family. Therefore, nonstandard amino acids are increasingly being used in the design of peptide ligands to introduce strong donor groups for metal complexation or to improve the sensitization of metal-ion emission.[12] Chelating moieties such as bipyridines, phenanthrolines, or hydroxyquinolines have been included in peptide sequences to obtain high-affinity metal binding sites for Zn^{2+} or other divalent d-block metals, either to design metal sensors[13,14] or to promote metal-assisted peptide self-assembly.[15] Amino acids bearing chelating side-chains adapted to hard cations, like γ-carboxyglutamate, have been inserted into peptides to induce folding through Ln^{3+} complexation.[16] Among metal-chelating amino acid side-chains, aminodiacetate groups have attracted our attention.[17–19] The corresponding residues are referred to as Ada_n (n being the length of the alkyl chain separating the peptide backbone from the aminodiacetate nitrogen). They have been shown to stabilize helical structures in synthetic peptides through divalent-metal-ion coordination.[20] The relationship between Ada_n-containing peptides and poly(aminocarboxylate) ligands is clear as Ada_n structures bear a tridentate chelating group analogous to the simple *N*-methyliminodiacetate (MIDA) ligand.

To design lanthanide–peptide complexes of enhanced stability with a ligating site embedded in the peptide structure, we decided to insert Ada_n unnatural amino acids into peptide sequences. As Ln^{3+} ions require high coordination numbers, several of these chelating units have to be used. However, the mere inclusion of chelating amino acids into an arbitrary peptide sequence is insufficient to achieve highly stable mononuclear complexes because the chelating side-chains show independent behavior. To overcome this difficulty, the propensity of peptide chains to adopt defined conformations in solution can be an asset to the design of coordinating sites involving two or more chelating side-chains. An analogy may be seen with the definition of metal-binding sites in metalloproteins by the spatial disposition of coordinating site-chains due to secondary and tertiary structure elements.[21]

In this paper we report the synthesis and solution studies of Ln^{3+} complexes with two hexapeptides (**P***n*) that incorporate two metal-binding amino acids Ada_n ($n=2$, 3). The two hexapeptides **P***n* can be viewed as models of poly(aminocarboxylate) ligands like EDTA or TMDTA with a peptide spacer instead of an alkyl spacer (see Scheme 1). In such systems the peptide backbone is used as a non-innocent spacer between the coordinating groups and was designed to favor a β-turn-containing structure. In such a turn, a hydrogen bond is usually present and the residues in positions i and $i+3$ are brought into close proximity.[22] This would bring the aminodiacetate side-chains closer into a disposition suitable for metal chelation. We demonstrate herein that the Ada_n side-chain length has a dramatic effect on the Ln^{3+} complexation properties. Whereas the two aminodiacetate moieties in the peptide **P³** behave as nearly independent subunits, the more compact ligand **P²** acts as an efficient hexadentate ligand of Ln^{3+} ions. Indeed, the formation of the stable mononuclear Ln**P²** complex benefits from peptide secondary structure stabilizing interactions.

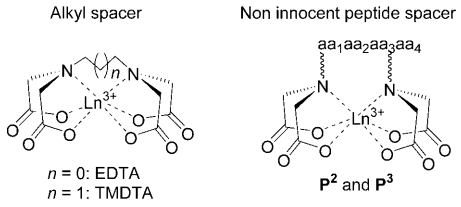

Scheme 1. Ln^{3+} chelates with poly(aminocarboxylate) hexadentate ligands and peptide ligands bearing two aminodiacetate groups.

Results and Discussion

Metal-chelating amino acid synthesis: The synthesis of Ada_n-containing peptides ($n=1$–4) was first reported by Hopkins and co-workers using *N*-Boc-Ada_n-OH synthons.[17] However, undesired side-reactions such as trifluoroacetate capping of the peptide were reported to occur using this Boc strategy. Other authors subsequently published the procedure for the synthesis of Ada_n-containing peptides using Fmoc-Ada_n-OH protected synthons.[18,19] However, the Fmoc group was introduced at the end of the synthetic sequence by using a temporary protection of the amine group. As a result, lengthy procedures involving multiple protection/deprotection steps were reported. The desired Fmoc-$Ada_n(t\mathrm{Bu})_2$-OH synthons were obtained in less than 10% overall yield from commercial products. Finally, no proof of the optical integrity of the protected synthetic amino acids was provided. We thus decided to develop new synthetic pathways to obtain Fmoc-$Ada_n(t\mathrm{Bu})_2$-OH ($n=2$, 3) by using Fmoc-protected intermediates in the first steps of the synthetic pathways.

The key steps in the synthesis of Fmoc-$Ada_2(t\mathrm{Bu})_2$-OH are a straightforward reductive amination/hydrogenolytic

debenzylation sequence starting from aldehyde **2**. The reductive amination procedure chosen ensures synthetic versatility as the nature of the amine to be coupled with aldehyde **2** could be easily varied. Protection of the carboxylic acid is necessary to facilitate purification of the synthetic products. Benzyl is an appropriate protecting group because of its ease of removal under catalytic hydrogenation conditions in the last step of the synthesis. The three-step synthetic pathway to **2** starting from commercially available L-homoserine (L-Hse) was reported by Rocchi and co-workers.[23] However, in the second step, Fmoc-Hse-OBn was isolated in only 48% yield probably because of the prompt lactonization of this intermediate. The synthesis of Fmoc-Hse-OBn was improved by conducting the benzylation in anhydrous DMSO using the conditions reported for the synthesis of Fmoc-Ser-OBn.[24] The crude Fmoc-Hse-OBn was oxidized, as published, under Swern conditions to give **2**.[23] Aldehyde **2** was then subjected to a reductive amination with di-*tert*-butyl iminodiacetate using $NaBH(OAc)_3$ as the reductant.[25] The resulting intermediate **3** was debenzylated to obtain the desired Fmoc-$Ada_2(tBu)_2$-OH. The synthetic procedure is summarized in Scheme 2.

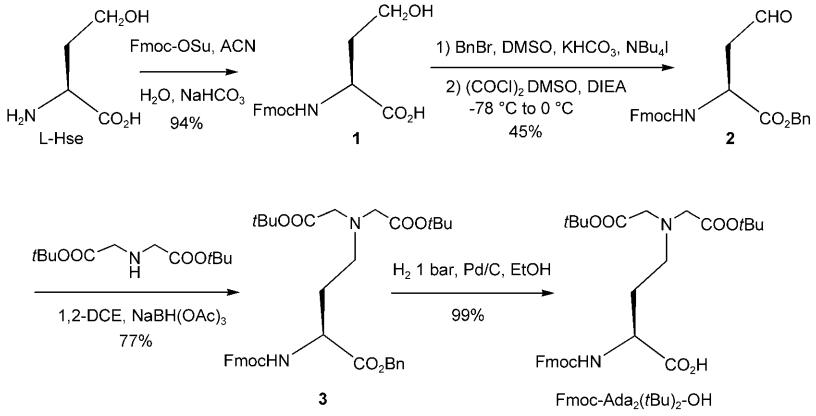

Scheme 2. Synthetic pathway to Fmoc-$Ada_2(tBu)_2$-OH.

Protected derivatives of L-ornithine (Orn), which already bear the Nε amine, are commercially available and the synthesis of Fmoc-$Ada_3(tBu)_2$-OH has previously been reported starting from this amino acid.[18] This synthesis was based on the difunctionalization of the Nε amine by a standard alkylation procedure. Again, the Fmoc group was introduced at the end of the synthetic sequence. We report herein a synthesis based on the same sequence of reactions that was conducted directly from Fmoc-Orn(Boc)-OH **4**[26] sparing tedious protection/deprotection steps (Scheme 3).

After quantitative Boc deprotection of the primary amine in a strong acid medium, nucleophilic substitution of the amine could be performed in moderate yield in mild basic conditions. The use of NBu_4I as a catalyst instead of poorly soluble NaI[18] greatly reduced the reaction time and the need to use an excess of electrophile, and led to an improvement in the yield of **5**. After final deprotection, Fmoc-$Ada_3(tBu)_2$-OH was recovered in a pure form.

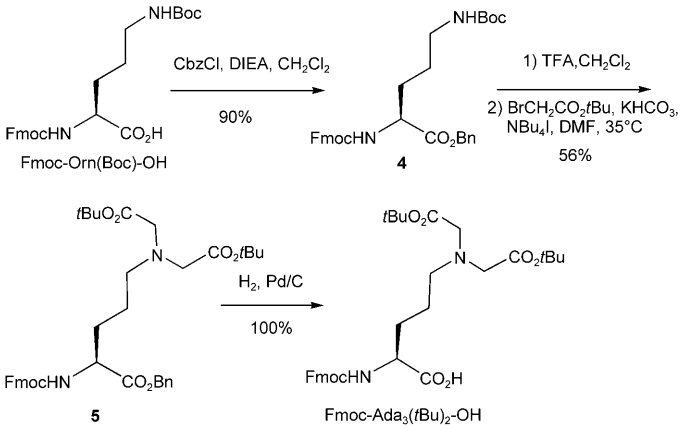

Scheme 3. Synthetic pathway to Fmoc-$Ada_3(tBu)_2$-OH.

Fmoc-$Ada_n(tBu)_2$-OH were obtained using mild conditions likely to preserve the enantiomeric integrity throughout the synthesis. However, enantiomeric purity is essential for peptide synthesis and must be confirmed. Coupling with a chiral amine (α-methylbenzylamine) either in an enantiopure or racemic form was performed and the coupling product was examined by ^1H NMR spectroscopy. Splitting of some signals (especially NH doublets) occurred only with the coupling product formed with the racemic amine, which indicates that the Fmoc-$Ada_n(tBu)_2$-OH synthons were enantiopure (see the Supporting Information for details).

Peptide design and synthesis: Two hexapeptides that incorporate two Ada_n chelating amino acids were designed with a peptide spacer (aa_2aa_3 = PG in Scheme 1) favoring a β-turn conformation. The design of short peptides natively forming β-turns is a difficult task.[27] Research efforts in that direction are motivated by the assumption that reverse turns are nucleating sites in protein-folding.[28] Even though it is not usually considered as a strong turn-inducer in linear peptides, the XPGX sequence is frequently encountered in type II β-turns in proteins.[22] Experimental data in solution[29] as well as molecular dynamics simulations[30] show that the turn structures are accessible in terms of conformational energy. Moreover, turns formed by L-prolylglycine spacers between coordinating amino acids have been found to tune metal-monitoring and induce some selectivity in fluorescent peptide probes in-

cluding artificial fluorophores.[31] Being cyclic, L-proline is unique among amino acids in promoting changes in protein backbone direction and in restricting the conformational space accessible to the peptide. In contrast, glycine possesses enough conformational freedom to comply with the Φ and Ψ backbone dihedral angle requirements of the type II β-turn structure and should also provide sufficient conformational elasticity for efficient metal coordination. A tryptophan residue was also inserted into the sequence of **P²** and **P³** to benefit from the antenna effect to sensitize Tb^{3+} luminescence. **P²** and **P³** may be viewed as minimal models to ascertain whether the Ada_n-PG-Ada_n sequences are compatible with the turn formation and to investigate the tuning of the complexation behavior by the L-prolylglycine spacer.

Starting from Fmoc-$Ada_n(tBu)_2$-OH and natural commercial amino acid derivatives, peptides **P²** and **P³** (see Scheme 4) were manually assembled by solid-phase peptide

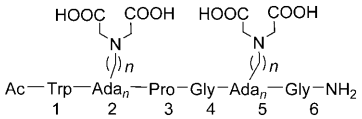

Scheme 4. Peptides **P²** ($n=2$) and **P³** ($n=3$) with sequence numbering.

synthesis (SSPS)[32] on the Rink amide MBHA resin using standard conditions (see the Experimental Section).

No significant byproducts were detected, which shows that the unnatural amino acids Fmoc-$Ada_n(tBu)_2$-OH displayed normal reactivity in the on-resin synthetic steps. Before resin cleavage, *N*-terminal acetylation was performed. As the choice of resin ensured the isolation of peptides as *C*-terminal amides, peptides were recovered after simultaneous resin cleavage and side-chain deprotection with both extremities protected. The deprotected peptides were obtained on a ~50 mg scale after preparative HPLC purification. Electrospray ionization mass spectrometry confirmed the identity of the purified peptides. **P²** and **P³** were further characterized by the standard combination of 1D and 2D ^{1}H NMR techniques:[33] COSY and TOCSY were used to establish intra-residue spin systems and ROESY allowed the assignment of signals. The spectra were assigned to only one species, which proves that no large-scale racemization processes occur in solution even though the Ada_n side-chains carry basic functions, that is, unprotected tertiary amines. The ROESY spectra of both peptides (500 MHz, 298 K) show no though-space correlations other than sequential ones. This, along with little dispersion of the NH amide and glycine Hα resonances, is indicative of flexible conformations in solution, as expected for linear oligopeptides (see Tables S1 and S2).

Peptide protonation: **P²** and **P³** were subjected to pH-metric titrations. They allowed the determination of two pK_a values >8 (amine functions) as well as two pK_a values <5 (acidic functions). The pK_a values are reported in Table 1 (see the Supporting Information for the experimental curves and details). Not all the carboxylic acids (pK_{a5} and pK_{a6} are <2) could be detected due to sample dilution. The values of pK_{a1} and pK_{a2} are important as they will be used later in this paper to calculate the stability constants from the conditional stability constants measured at pH 7. The first pK_a of **P³** has the same value as the first pK_a of MIDA, which indicates no effect of the peptide backbone. Chain-shortening from three to two carbon atoms lowers the amine pK_a values by 0.8 log units. This can be attributed to the withdrawing effect of the peptide backbone amide functions through the short side-chains of Ada_2 in **P²**.

Table 1. Equilibrium constants of **P²** and **P³**.[a]

Equilibrium constants	**P²**	**P³**	**MIDA**[b]
pK_{a1}	8.8(1)	9.6(2)	9.59
pK_{a2}	8.2(1)	8.9(2)	2.32
pK_{a3}	2.8(1)	2.9(1)	≈1.9
pK_{a4}	≈2	2.0(1)	–
$\log\beta_{11}^{pH7}$ (TbL)	9.1(5)	5.4(3)	4.5
$Log\beta_{21}^{pH7}$ (Tb_2L)	–	≈9	–
$\log\beta_{110}$ (TbL)	12.1(5)	9.9(3)	7.11

[a] $I=0.1$ M (KCl) at 298 K. β_{x1}^{pH7} represents the conditional stability constants at pH 7 and β_{110} the stability constants. [b] See ref. [34].

Potentiometry requires large amounts of material, especially for the reliable determination of metal-complex stability constants. Therefore, it is not the technique of choice for studying the metal complexes of **P²** and **P³**. We report hereafter the characterization of the **P*n***–Ln interaction in solution by other physicochemical techniques.

Mass spectrometry of EuP*n*: Electrospray mass spectrometry (ES-MS) provides a qualitative insight into the speciation in solution of the Ln^{3+} complexes of **P²** and **P³**. This method is the most suitable of the MS techniques for the study of metal–ligand complexes in solution.[35]

Mass spectra were recorded for **P²** and **P³** in the presence of $EuCl_3$. The most significant peaks observed in the positive and negative ionization experiments are reported in Table 2. For **P²** only signals corresponding to mononuclear

Table 2. Significant peaks observed in the (+)- or (−)ESI mass spectra of 60 μM peptide solutions in $AcONH_4$ buffer (20 mM, pH 7) in the presence of $EuCl_3$.[a]

		(+)ESI	(−)ESI
P²	+0.5 Eu^{3+}	889.4 $[\mathbf{P^2}+H]^+$	887.3 $[\mathbf{P^2}-H]^-$
		445.2 $[\mathbf{P^2}+2H]^{2+}$	443.2 $[\mathbf{P^2}-2H]^{2-}$
		1039.3 $[\mathbf{P^2}-2H+Eu]^+$	1037.3 $[\mathbf{P^2}-4H+Eu]^-$
		520.3 $[\mathbf{P^2}-H+Eu]^{2+}$	518.2 $[\mathbf{P^2}-5H+Eu]^{2-}$
	+1.0 Eu^{3+}	1039.3 $[\mathbf{P^2}-2H+Eu]^+$	1037.3 $[\mathbf{P^2}-4H+Eu]^-$
		520.3 $[\mathbf{P^2}-H+Eu]^{2+}$[b]	518.2 $[\mathbf{P^2}-5H+Eu]^{2-}$[b]
	+2.0 Eu^{3+}	[c]	[c]
P³	+0.5 Eu^{3+}	917.6 $[\mathbf{P^3}+H]^+$	915.5 $[\mathbf{P^3}-H]^-$
		459.5 $[\mathbf{P^3}+2H]^{2+}$	457.3 $[\mathbf{P^3}-2H]^{2-}$
		1067.5 $[\mathbf{P^3}-2H+Eu]^+$	1065.3 $[\mathbf{P^3}-4H+Eu]^-$(weak)
		534.4 $[\mathbf{P^3}-H+Eu]^{2+}$	532.3 $[\mathbf{P^3}-5H+Eu]^{2-}$ (weak)
	+1.0 Eu^{3+}	[d]	[d]
	+2.0 Eu^{3+}	608.3 $[\mathbf{P^3}-4H+2Eu]^{2+}$[c]	[c]

[a] Sodium (+22/z) and potassium (+38/z) adducts were also detected. [b] Nearly total disappearance of the signals of the free peptide. [c] The same peaks as 1.0 equiv. [d] The same peaks as 0.5 equiv; no disappearance of the signals of the free peptide.

species were detected. With 1 equiv or excess Eu^{3+}, signals associated with the uncomplexed peptide disappeared from the spectra. **P³** showed different behavior. In comparison with **P²**, the intensity ratio of the complexed/uncomplexed peptide signals is smaller in each experiment. Signals of the free peptide were detected even with a two-fold excess of $EuCl_3$. More interestingly, a Eu_2**P³** species was detected in the presence of 2 equiv $EuCl_3$.

Strikingly, the major peaks observed in a competition experiment ([**P²**]=[**P³**]=[Eu]) correspond to complexed **P²** and uncomplexed **P³** (Figure 1). Mass spectrometry is not a quantitative analysis technique. However, in the case of similar molecules like the peptide ligands **P²** and **P³**, it is likely that the relative intensities of signals belonging to species of the same charge reflect abundances in solution. The results of this competition experiment thus indicate that **P²** is a stronger ligand than **P³** towards Eu^{3+}.

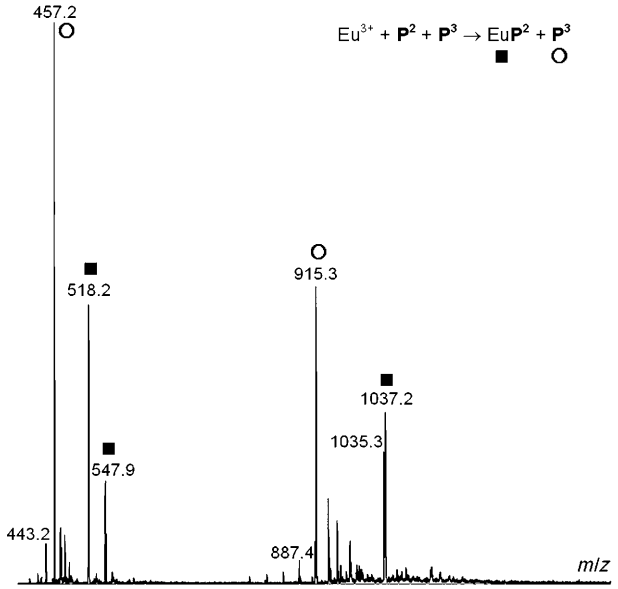

Figure 1. (−)-ESI mass spectrum of a solution containing **P²**, **P³**, and $EuCl_3$ (30 μM) in $AcONH_4$ buffer (20 mM, pH 7). See Table 2 for peak assignments (m/z = 547.9 $[\mathbf{P^2}-4H+Eu+AcO]^{2-}$, molecular association).

Circular dichroism studies: Circular dichroism (CD) titrations were performed to monitor the modification in the dichroic signal in the region of the amide bands upon the addition of Tb^{3+} to **P²** and **P³** solutions. The use of Tb^{3+} was chosen for consistency with luminescence studies reported hereafter. CD spectra can reveal the presence of secondary structure elements in peptides or proteins. However, in contrast with the well-defined CD signature of β-sheets and α-helices, the identification of turns by their CD signature alone is usually not reliable.[36,37] Indeed, the CD signature of type II β-turns (type B spectrum in Woody's theory) may not be seen in linear peptides: The mean molar ellipticity per residue in such a turn (including a positive band at around 200 nm) is lower by a factor of four in comparison with that of a carbonyl amide in a random coil environment (strong negative band at 195 nm).[37] Furthermore, aromatic side-chains such as Trp indoles could contribute to far-UV CD and thus complicate spectral interpretation.[38]

As anticipated from the results of the ES-MS experiments, the two peptides show different behavior. For **P²**, the addition of up to 1 equiv Tb^{3+} caused a change in the CD signal clearly associated with an isodichroic point at 208 nm (Figure 2, top). No further ellipticity changes were observed upon the addition of excess Tb^{3+}. In contrast, a two-phase change in the dichroic signal was detected for the **P³**–Tb system (Figure 2, bottom). Up to 1 equiv of Tb^{3+}, a decrease in the negative ellipticity at 199 nm was observed associated with an isodichroic point at 214 nm. Above 1 equiv, the formation of a second species was detected with a slow decrease in the negative ellipticity at 195 nm. For this second process, no plateau was reached even with a large excess of Tb^{3+}, which indicates that the second process is not completed even with a 10-fold excess of the metal ion. These results are in agreement with the speciation model suggested

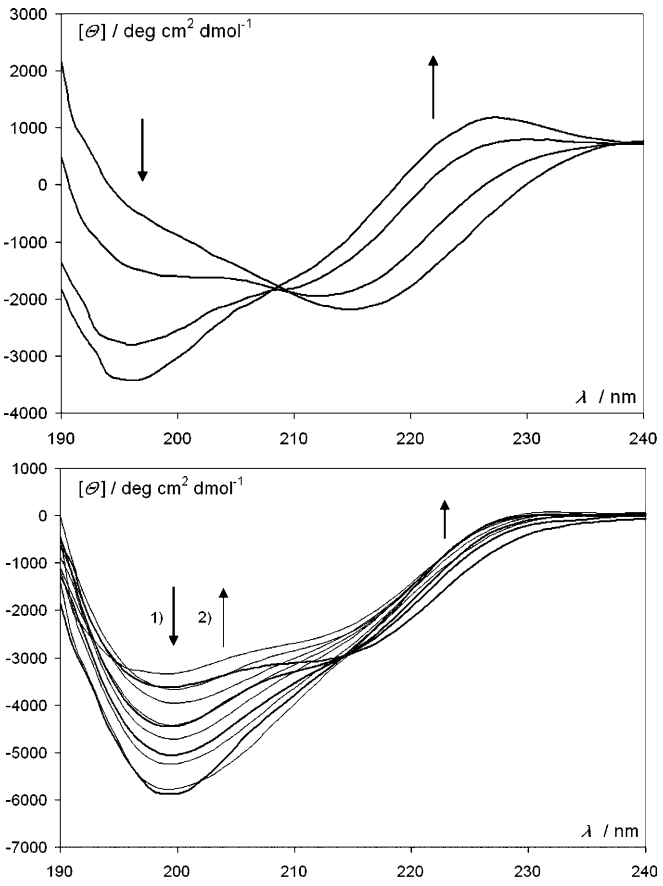

Figure 2. Changes in the far-UV CD signals of **P²** (top) and **P³** (bottom) upon addition of $TbCl_3$ in water (pH 7). Peptide concentration about 20 μM. **P²**: titration with 0.33 equiv aliquots of Tb^{3+} until 1 equiv. **P³**: titration with 0.33 equiv aliquots of Tb^{3+} until 2 equiv, then 3, 5, 7 equiv. 1) Spectral traces up to 1 equiv (highlighted). 2) Spectral traces for 1.33–7 equiv.

by the ES-MS experiments: Tb$\mathbf{P^2}$ is the only metallic species formed in water (pH 7) whereas the mononuclear complex Tb$\mathbf{P^3}$ is transformed into a second complex, $Tb_2\mathbf{P^3}$, in the presence of an excess of the metal ion.

Tryptophan fluorescence and Tb^{3+} phosphorescence: Owing to the antenna effect, in the present case Tb^{3+} luminescence sensitization by energy transfer through Trp indole absorption at around 280 nm, the Tb–peptide complexes could be detected at concentrations as low as 0.5 μM. Reliable titrations could be performed at concentrations as low as around 10 μM peptide. $TbCl_3$ titrations of solutions of peptides dissolved in HEPES buffer (10 mM, pH 7) were performed. The build-up of the Tb-centered $^5D_4 \rightarrow {}^7F_J$ bands ($J=3$–6) and the modification of the Trp fluorescence were monitored.

The intensity of the Trp fluorescence signal increased significantly up to 1 metal equiv during the Tb titration (+34%) with $\mathbf{P^2}$. A modest redshift in the emission maxima (from 349 to 351 nm) was also observed. Titrations conducted with the nonluminescent lanthanum ion La^{3+} instead of Tb^{3+} gave very similar results: +40% intensity, 2 nm redshift (see Figure 3 for La and Figure S4 for Tb). Even though the photophysics of tryptophan side-chains in peptides is a rather complex subject,[39] this enhancement of the Trp luminescence may indicate that the Trp side-chain is in a more rigid environment in the complex in comparison with the free peptide and/or that the tryptophan is less accessible to water in the complexes. This effect largely exceeds in magnitude the Trp-to-Tb^{3+} energy transfer, which is expected to lead to a decrease in the Trp luminescence intensity. Indeed, the Trp-to-Tb^{3+} transfer is not an efficient process.[40] The intensity of the Trp emission also increased during the Tb titration with $\mathbf{P^3}$ (+15%), as it did in titrations with nonluminescent La^{3+} (Figure S6, +16%). The increase is less marked than for $\mathbf{P^2}$, which may indicate differences in the tryptophan environment in the two complexes.

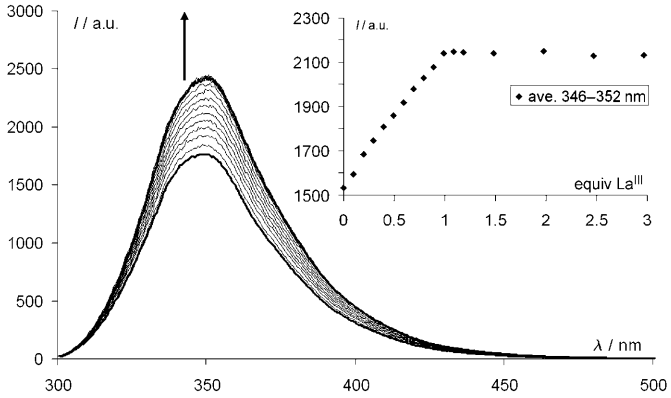

Figure 3. Increase in the Trp-centered emission of $\mathbf{P^2}$ (76.4 μM) upon addition of $LaCl_3$ in HEPES buffer (10 mM, pH 7, 0.1 M KCl). The spectral traces with 0 and 1 equiv Tb are shown as bold lines. Inset: Variation of the intensity of the peak maximum (average intensity 346–352 nm) with La.

The build-up of the Tb-centered luminescence through excitation of the tryptophan moiety shows a sharp end-point for the $\mathbf{P^2}+Tb^{3+}$ titration, which is characteristic of a large stability constant (Figure 4). The binding curves recorded with $\mathbf{P^3}$ are much smoother (Figure 5), which indicates a lower affinity of this latter peptide for Tb^{3+}. In contrast to the CD titrations, the binuclear complex $Tb_2\mathbf{P^3}$ is not directly viewed in the spectral evolution above 1 equiv Tb^{3+} because the luminescence spectra of Tb$\mathbf{P^3}$ and $Tb_2\mathbf{P^3}$ may be very similar.

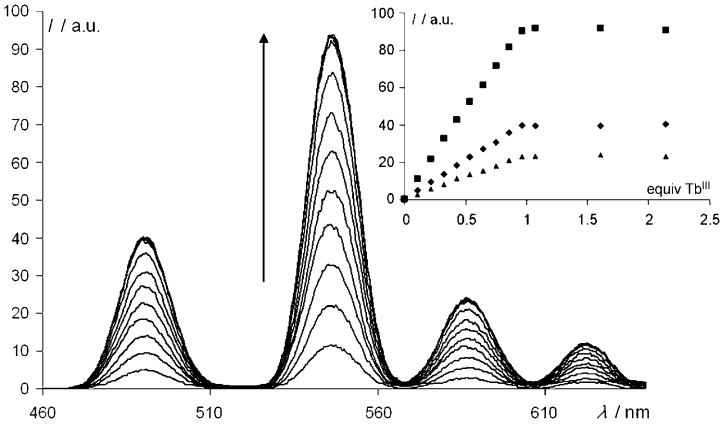

Figure 4. Build-up of the Tb-centered emission during the titration of $\mathbf{P^2}$ (49.5 μM) with $TbCl_3$ in HEPES buffer (10 mM, pH 7, 0.1 M KCl). Inset: Variation of the intensities of the peak maxima with Tb (◆: 490 nm; ■: 545 nm; ▲: 587 nm).

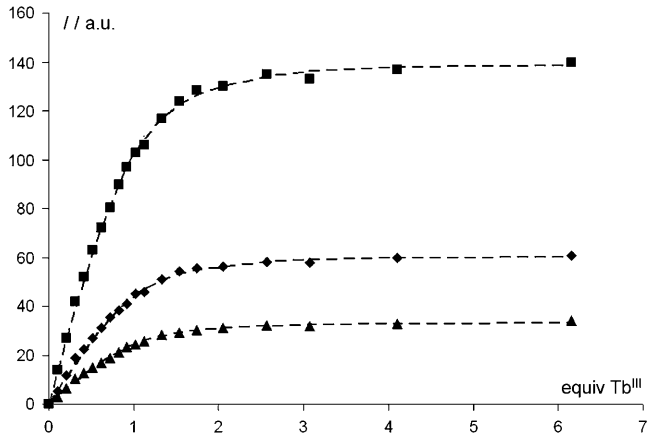

Figure 5. Build-up of the Tb-centered emission at selected wavelengths during the titration of $\mathbf{P^3}$ (19.7 μM) with $TbCl_3$ in HEPES buffer (10 mM, pH 7, 0.1 M KCl). Dashed lines represent calculated data with $\log\beta_{11}^{pH7} = 5.4$ (◆: 490 nm; ■: 545 nm; ▲: 587 nm).

The luminescence lifetimes of Tb^{3+} in the Tb$\mathbf{P^n}$ complexes in H_2O and D_2O were measured to obtain the hydration number q_{Tb} of these complexed ions using the empirical equations of Horrocks and Sudnick[41] or of Parker and coworkers.[42] To avoid underestimating the luminescence lifetimes in D_2O because the peptides are accompanied by H_2O hydration molecules, τ_{D_2O} was determined as the extrapolat-

ed limit of the luminescent decay rates in solutions of increasing D_2O molar fractions tending to a H_2O-free solution (Figure S7). The experimental values of τ_{H_2O} and τ_{D_2O} (Table 3) for Tb**P²** and Tb**P³** give a hydration number close

Table 3. Luminescence lifetimes and calculated hydration numbers for the Tb**P***n* complexes.

Peptide	τ_{H_2O}/ms	τ_{D_2O}/ms	q[a]	q[b]
P²	1.11(1)	3.71(3)	2.9(1)	2.8(1)
P³	1.01(1)	2.75(3)	2.8(1)	2.6(1)

[a] Calculated according to ref. [42]. [b] Calculated according to ref. [42].

to 3 for both peptide complexes. These values compare well with those of the $[Tb(EDTA)(H_2O)_q]^-$ complex, which were found to be 2.8.[42,43] They are thus consistent with both peptides behaving as hexadentate ligands. Different denticity is thus not the origin of the different stabilities of the mononuclear Tb**P***n* complexes.

Stability constants: Tb^{3+} luminescence titrations are particularly suitable for obtaining quantitative information about the stability constants of the complexes in solution. For **P³**, titrations conducted in diluted peptide solutions ([**P³**] $\approx 20\,\mu M$) at pH 7 could be interpreted as the formation of only one complex, Tb**P³**, or of the two species, Tb**P³** and Tb_2**P³**. These two models give the same conditional stability constant for the mononuclear complex within experimental error: $\log\beta_{11}^{pH\,7} = 5.4(3)$. Figure 5 shows the good agreement between experimental and calculated data for the most intense terbium emission bands. In contrast, titrations conducted at higher **P³** concentrations ($>100\,\mu M$) could not be fitted with only one metallic complex and the formation of the binuclear complex Tb_2**P³** had to be taken into account in the fitting procedure, with $\log\beta_{21}^{pH\,7} \approx 9$. Owing to the limited change in the observed signal, precise determination of $\log\beta_{21}^{pH\,7}$ from the experimental data was not possible.

The analysis of the titration data obtained with **P²** concentrations in the range 20–200 μM revealed that the **P²**–terbium system could be completely described by the total formation of Tb**P²** between 0 and 1.0 equiv of added metal (Figure 4). Direct titrations did not allow the stability constants for Tb**P²** to be determined because the signal-to-noise ratio was not sufficiently favorable for dilute samples to detect significant amounts of the free peptide in the presence of a stoichiometric quantity of Tb^{3+}. Nitrilotriacetic acid (NTA) was chosen as a competitive ligand for **P²** because the pK_as and the stability constants of the mononuclear Tb(NTA) and binuclear $Tb(NTA)_2$ complexes are known. Conditional stability constants at 298 K, pH 7.0, and 0.1 M KCl can be calculated from published data: $\log\beta_{11}^{pH\,7} = 8.8(2)$ and $\log\beta_{12}^{pH\,7} = 15.6(3)$.[34] Tb^{3+} luminescence spectra were recorded during the titration of Tb**P²** with NTA. The data could be fitted with a simple model that involves the displacement of Tb from the peptide ligand and the formation of nonluminescent Tb(NTA) and $Tb(NTA)_2$ (Figure 6). Knowing the conditional stability constants of the latter complexes, the stability constant of Tb**P²** was determined to be $\log\beta_{11}^{pH\,7} = 9.1(5)$. Uncertainties arise in approximately equal parts from experimental errors in the competition experiments and from the uncertainties in the published Tb–NTA stability constants.

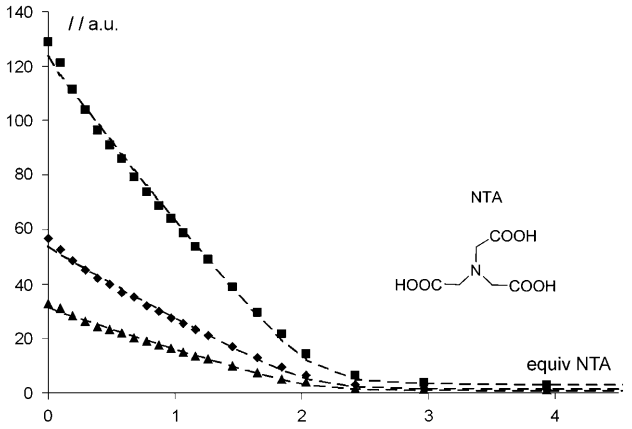

Figure 6. Decline of the Tb-centered emission at selected wavelengths during the titration of a solution containing **P²** (91.1 μM) and $TbCl_3$ (91.1 μM) with nitrilotriacetic acid in HEPES buffer (10 mM, pH 7, 0.1 M KCl). Dashed lines represent calculated data with a conditional stability constant $\log\beta_{11}^{pH\,7} = 9.1$ for the Tb**P²** complex (◆: 490 nm; ■: 545 nm; ▲: 587 nm).

The values of the conditional stability constants at pH 7 are reported in Table 1. These values determined at a specific pH depend on the basicity of the ligands. Therefore, to compare the stabilities of the two Tb**P***n* complexes, the stability constants (Table 1) were calculated from the conditional values at pH 7 and the pK_as of the two peptide ligands. The Tb**P²** complex is found to be two orders of magnitude more stable than the Tb**P³** complex ($\Delta\log\beta_{110} \approx 2.2$), although the two peptides act as hexadentate ligands of lanthanide ions. Indeed, the Tb^{3+} ion has the same hydration number in the two mononuclear complexes. Furthermore, the formation of the binuclear adduct with **P³** clearly evidences the tendency of **P³** to act as a bis(tridentate) ligand and to complex two metal ions. The Tb**P³** complex shows nearly the same stability as hexadentate poly(aminocarboxylate) ligands with long alkyl chains (Scheme 1, $n = 2$–4, $\log\beta_{110} = 9.5$–10.8).[34] The latter do not provide significant chelate effects between the two aminodiacetate moieties and benefit only from the entropic stabilization because of the presence of the two tridentate units in the same molecule.

In contrast, [Tb(EDTA)] or [Tb(TMDTA)] complexes (Scheme 1, $n = 0$, 1, respectively) show very large chelate effects due to the formation of five- or six-membered chelate rings through the coordination of the two nitrogen atoms. Although not as marked as for these ligands, Tb**P²** shows a significant stabilization of two orders of magnitude in comparison with ligands bearing independent aminodiacetate moieties, even though the coordinating nitrogen atoms are separated by 14 atoms. This effect is a result of peptide secondary structure elements, such as, β-turn formation, as demonstrated by solution NMR studies and presented in the following paragraphs.

NMR signature of LnP^n: ^{1}H NMR spectroscopy was used to investigate the effect of Ln^{3+}-binding on the backbones of peptides **P^2** and **P^3**. To detect the changes in the CH region (1–5 ppm) clearly, the study was performed in D_2O. The pD was adjusted to a value of 7 for consistency with the luminescence and CD studies. Attempts to use lanthanide-induced shifts and relaxation[4,44] to investigate the solution structure of paramagnetic lanthanide complexes of **P^2** and **P^3** were unsuccessful. The NMR spectra of Eu^{3+} and Yb^{3+} complexes show very broad proton resonances because of intramolecular dynamics, as already observed for tetrapodal ligands with soft donor nitrogen groups.[45] More details on the structures of the complexes were obtained from the NMR data of the diamagnetic lanthanum complexes.

The addition of $La(OTf)_3$ to a solution containing **P^3** resulted in general line-broadening of the spectrum as well as small modifications in the chemical shifts of the observed signals (Figure 7). The signals that experienced the greatest

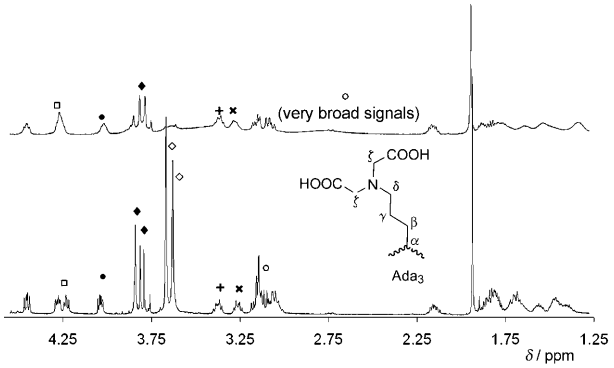

Figure 7. Partial ^{1}H NMR spectra of **P^3**+$La(OTf)_3$ (D_2O, 500 MHz, 298 K, pD 7, [**P^3**] = 0.99 mM): bottom) 0 equiv La^{3+}, top) 1.0 equiv La^{3+}. The following signals are marked: Open symbols for Ada_3 residues (Hα: □; Hδ: ○; Hζ: ◇); filled symbols for other residues (Pro3 Hα: ●; Gly4 and Gly6 Hα: ◆; Pro3 Hδ × and + symbols).

shift and the most severe line-broadening were the side-chains of the Ada_3 residues ($C\zeta H_2 \gg C\delta H_2 > C\gamma H_2$). However, the peptide backbone signals are virtually unmodified upon lanthanum coordination (Figure 7 and Tables S3 and S4). This can be interpreted as an indication of limited conformational rearrangement upon coordination.

In contrast to **P^3**, the addition of $La(OTf)_3$ to a solution containing **P^2** resulted in marked changes in the NMR spectra. The addition of less than 1 equiv of $La(OTf)_3$ resulted in the observation of two sets of signals: Those of the unreacted apopeptide and a new set of signals belonging to the mononuclear complex La**P^2**. The signals of the complex were unambiguously assigned with a 2D EXSY spectrum of a sample containing 0.5 equiv $La(OTf)_3$. The ^{1}H NMR spectra are shown in Figure 8 and the full NMR assignment is given in Tables S5 and S6. Line-broadening was observed in the side-chains of the coordinating amino acids ($C\varepsilon H_2 \gg C\gamma H_2 > C\beta H_2$), but this effect was less pronounced than for **P^3**. More interestingly, the signals of protons far from the

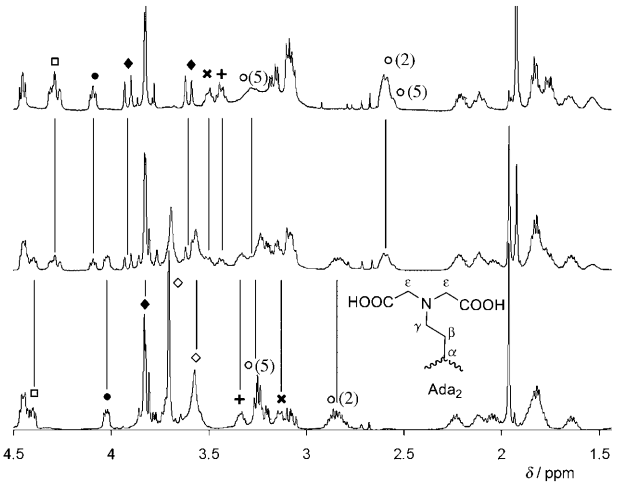

Figure 8. Partial ^{1}H NMR spectra of **P^2**+$La(OTf)_3$ (D_2O, 500 MHz, 298 K, pD 7, [**P^2**] = 1.05 mM): bottom) 0 equiv La^{3+}, middle) 0.5 equiv La^{3+}, and top) 1.0 equiv La^{3+}. The following signals are marked: Open symbols for Ada_2 residues (Hα: □; Hγ: ○; Hε: ◇); filled symbols for other residues (Pro3 Hα: ●; Gly4 Hα: ◆; Pro3 Hδ (pro-*R*): ×; Pro3 Hδ (pro-*S*): +).

coordination site showed significant modifications. In particular, the signals of the Pro3 Hα and Hδ atoms experience changes in chemical shifts of up to 0.36 ppm. Moreover, the glycine Hα region is clearly modified. A poorly resolved multiplet accounting for all four Gly Hα atoms is observed in the spectrum of the apopeptide, whereas the protons of one of the glycines in the La**P^2** complex give rise to a pair of doublets.

However, at this point it was not possible to attribute the split signals to one of the glycines in particular because of the overlapping of all the glycine Hα atoms in the apopeptide spectrum. The ^{1}H WATERGATE NMR spectrum of La**P^2** in H_2O/D_2O (9:1, v/v) at pH 7 shows the signals of the NH amide protons at 278 K (Figure S8). 2D NOESY and ROESY spectra recorded at this temperature allowed us to confirm the signal assignment and to assign unambiguously the glycine resonances in the complex. The Gly4 Hα atoms in La**P^2** correspond to a pair of well-separated (0.32 ppm) doublets, which indicates that this glycine is in a well-defined environment. The most significant changes in the NMR signal are thus in the Pro3-Gly4 region of the spectrum, that is, the spacer between coordinating residues. These observations could indicate that a transition from an open to a turn-containing structure occurs upon complexation. Such changes prompted us to determine the structure of the La**P^2** complex by an NMR study

NMR structure of LaP^2: The objective of this structural analysis was to determine if the lanthanum complexation by **P^2** is associated with characteristic elements of peptide secondary structure. Indeed the presence or absence of secondary structure elements has been invoked to explain the relative stabilities of metal complexes.[13]

The solution structure of the La**P²** complex (3.53 mM) was investigated by 1D and 2D ^{1}H NMR experiments in H_2O/D_2O (9:1, v/v) at pH 7 and 278 K. The temperature of 278 K was chosen for the structural study for two reasons. First, the ^{1}H NMR WATERGATE spectrum in H_2O/D_2O (9:1, v/v) displayed only low intensity residual amide NH signals at 298 K. These signals partly recovered their intensity at 278 K. Secondly, preliminary experiments showed that signals of very low intensity were detected in NOESY experiments at 298 K due to an unfavorable $\omega_0\tau_c$ product, as is common for medium-sized molecules.[46] The product $\omega_0\tau_c$ can be increased by lowering the temperature and therefore the solvent viscosity and large negative NOE correlations could be obtained at 278 K. A total of 92 NOE restraints obtained from the 2D-NOESY spectrum were used in structural calculations with 23 intra-residue NOEs and 47 sequential NOEs as well as 22 medium-range NOEs (i.e., between residues i and $i\pm2$ or $i\pm3$). Correlations of the barely assignable and very broad signals of Hε (CH_2COO^-) were not used in the calculations. Of the medium-range NOEs, 16 correlations were ascribed to contacts between the Pro pyrrolidine ring and the indole aromatic side-chain of Trp. The *trans* conformation of the peptide bond with proline is evidenced by the presence of short contacts: d(Ada$_2$2 Hα, Pro3 Hδ1) = d(Ada$_2$2 Hα, Pro3 Hδ2) = 2.2 Å. The Ada$_2$ProGlyAda$_2$ motif shows two characteristic features of a type II β-turn structure: A *cis* relationship between Gly4 NH and Pro3 Hα (2.3 Å) and weak NOE cross-peaks between Gly4 NH and Pro4 Hδ1 (4.7 Å) and Hδ2 (4.8 Å). Unfortunately, no strong correlations between the i and $i+3$ side-chains could be detected because the identical nature of the Ada$_2$ residues results in signal overlap. The turn structure was, however, deduced by the observation of a number of short- and medium-range NOE correlations in the Ada$_2$GPAda$_2$ region.

Fifty structures were calculated by using CNSsolve 1.1[47] with standard refinement protocols using custom topologies and parameter files for the Ada$_2$ residues and for the lanthanum coordination sphere (see the Experimental Section). A superimposition of the 10 lowest-energy structures is shown in Figure 9. In these structures the Ada$_2$ProGlyAda$_2$ motif forms a type II β-turn. The carbonyl group of Ada$_2$2 and the NH group of Ada$_2$5 are linked by a hydrogen bond with an angle between the donor proton, the donor atom, and the acceptor atom of 170(7)° and an average O–N distance of 3.01(7) Å, which is close to the optimum for such a bond.[22] As seen in Figure 9 (middle), the peptide backbone and the Trp side-chain are rather well-defined except for Gly6, whereas the Ada$_2$ side-chains, especially that of Ada$_2$5, are more flexible (Figure 9, right).

The efficiency of the energy transfer between the donor (tryptophan) and the acceptor (Tb^{3+}) is described by a dipole–dipole mechanism and is strongly related to the distance that separates the donor and the acceptor.[40] In the LBT structures reported in the literature this distance is approximately 7 Å because the backbone carbonyl of the tryptophan residue is coordinated to the terbium ion.[10,48] In the 10 lowest-energy structures of the complex LaP^2, the La^{3+} ion is located 8.7(±0.4) Å from the center of the indole. The distance between the acceptor and the donor is slightly larger in La**P²** than in the LBTs, mainly because the tryptophan carbonyl is not coordinated to the metal center. Nevertheless the complex La**P²** was clearly detected in the micromolar range under our experimental conditions.

The backbone adopts a U-shaped conformation and the Trp–Pro hydrophobic interaction is clearly apparent in the calculated structures: The average separation between the centroids of the Trp benzene and the Pro five-membered ring is 4.36(1) Å with a tilt angle of 9.0(5)°. This hydrophobic interaction is likely responsible for the significant enhancement of the Trp fluorescence upon lanthanide complexation mentioned in a previous section. Trp–Pro stacking has been recognized as a stabilizing interaction in peptides and the interaction observed in La**P²** between the nearly coplanar proline and benzenic rings is the most frequently encountered case for Trp-X-Pro sequences.[49] In summary, the La**P²** complex adopts a U-shaped structure with an "upper face" devoted to lanthanum coordination and a "lower face" involved in the hydrophobic interaction.

Solution structures of peptide–metal complexes with cations displaying strong and directional metal coordination bonds (for instance, mercury[50] and palladium[51]) have been obtained by NMR studies. For these types of metal cations secondary structure elements are enforced by metal coordination. In contrast to these metals, Ln^{3+} coordination bonds are weaker and not directional. This is in agreement with the flexible behavior of the Ada$_2$ side-chains in the complex.

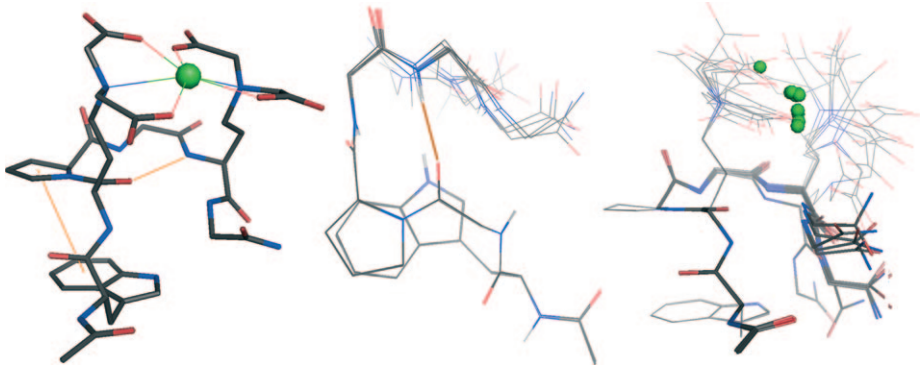

Figure 9. NMR structure of La**P²**. Left: lowest energy ball-and-stick structure, stabilizing interactions represented as orange lines; Middle: superimposition of the backbones and Trp side-chains of the 10 lowest-energy structures; Right: superimposition of the 10 lowest-energy structures (backbone and Trp side-chain: sticks, coordinating side-chain: lines).

It is also for this reason that lanthanide–peptide complexes are usually poorly defined structurally and indeed only one NMR structure of a La–peptide complex has been published.[48] Lanthanum coordination by **P²** and the establishment of the $Ada_2$5 NH···OC $Ada_2$2 hydrogen bond as well as the Trp–Pro hydrophobic interaction may thus better be viewed as occurring synergistically. These interactions can reduce the unfavorable conformational energy terms associated with peptide backbone reorganization upon complexation. Turn formation and hydrophobic Trp–Pro contact occur only in Ln**P²** and may be considered as the structural origin of the marked difference in stability between the Ln^{3+} complexes of **P²** and **P³**.

Conclusions

Metal-chelating unnatural amino acids bearing aminodiacetate moieties (Ada_n) have been introduced into peptide sequences to obtain peptide ligands with enhanced affinity for trivalent lanthanide ions. The two $AcWAda_nPGAda_nGNH_2$ hexapeptides differ only in the length of the Ada_n side-chains (two carbon atoms for **P²** and three for **P³**). Moreover, these peptides contain an XPGX sequence as a non-innocent spacer between the two metal-chelating amino acids. This motif is known to favor a type II β-turn, which should bring closer the two Ada_n subunits to allow hexadentate coordination of Ln^{3+} ions. These two peptides were satisfactorily obtained by solid-phase peptide synthesis using the classic Fmoc/*t*Bu strategy from commercially available protected natural amino acids and the unnatural amino acid derivatives Fmoc-$Ada_n(tBu)_2$-OH. The latter were synthesized in the enantiopure form with overall yields of 32 and 50% for $n=2$ and $n=3$, respectively.

The complexation of Ln^{3+} by **P²** and **P³** was studied by complementary analytical methods like ES-MS, CD, luminescence, and solution NMR spectroscopy. These studies demonstrate that the Ada_n side-chain length has a dramatic effect on the complexation properties of the peptides towards Ln^{3+} ions. Indeed, the more flexible **P³** forms a mononuclear complex of low stability, which tends to transform into a binuclear species in the presence of an excess of the metal ion. In this latter complex, the two binding aminodiacetate moieties act as independent chelating groups. The stability constant of Tb**P³** is $10^{9.9}$, which is similar to the constants obtained with poly(aminocarboxylate) ligands with long alkyl spacers between two aminodiacetate groups ($n \geq 2$ in Scheme 1). In the complexes of these ligands, the large chelate rings formed through the coordination of the two nitrogen atoms do not significantly stabilize the complexes. Therefore we do not expect a peptide secondary structure to contribute significantly to the stability of the Ln**P³** complex.

Interestingly, the more compact peptide **P²** provides more stable Ln^{3+} complexes with the exclusive formation of the mononuclear Ln**P²** adduct. The stability constant is two orders of magnitude higher ($10^{12.1}$) than that measured for **P³**, which demonstrates that the two Ada_n subunits are not independent. Although the solution NMR spectra indicate no structure elements for La**P³**, a well-defined structure is clearly observed in the 1D and 2D ^{1}H NMR spectra of La**P²**. Indeed, the features characteristic of a peptide secondary structure are apparent in the NOESY and ROESY spectra of La**P²**: The Ada_2PGAda_2 motif adopts a conformation with a type II β-turn showing a perfect hydrogen bond between the carbonyl of $Ada_2$2 and the NH group of $Ada_2$5 and a hydrophobic interaction between the aromatic group of the tryptophan residue and the aliphatic proline ring. This complex adopts a U-shaped structure with an "upper face" devoted to lanthanide coordination and a "lower face" involved in the hydrophobic interaction. These elements of peptide secondary structure contribute to the stability of the La**P²** complex and explain the marked difference in the stabilities of Ln**P²** and Ln**P³**. Although the two aminodiacetate moieties act nearly like independent tridentate binding groups in **P³**, synergistic effects of Ln^{3+} complexation, β-turn formation, and the Trp–Pro hydrophobic contact for the more compact peptide **P²** provide an efficient lanthanide-binding peptide. In addition, the withdrawing effect of the amide groups of the peptide backbone on the amine nitrogen atoms of **P²** lowers the two tertiary amine pK_a values, which leads to a conditional stability constant of $10^{9.1}$ at pH 7. This value can be compared with previously reported values for peptides based exclusively on natural amino acids that are in the range of 10^6–10^7.

To conclude, this study demonstrates that a subtle interplay between the basicity, the compactness of the ligand (lengths of the side-chains bearing the chelating groups), and the secondary structure of the peptide backbone can lead to lanthanide–peptide complexes of enhanced stability in comparison with peptides containing only natural amino acids. In these complexes, the ligating site is embedded in the peptide structure. Systems with higher denticity with scaffolds similar to **P²** should lead to even more stable Ln^{3+} peptide complexes.

Experimental Section

General: Reagents and solvents were purchased from Aldrich and Novabiochem and used without further purification unless specified. The organic products were characterized by NMR spectroscopy by using a Varian Mercury 400 MHz spectrometer at 298 K. Analytical and preparative peptide RP-HPLC were performed with LaChrom and LaPrep systems (see text for details). Specific rotations $[\alpha]$ are given in 10^{-1} deg cm^2 g^{-1}, with the concentration c in g per 100 mL.

Abbreviations: Ac_2O, acetic anhydride; DMF, *N*,*N*-dimethylformamide; DIEA, *N*,*N*-diisopropylethylamine; DTT, dithiothreitol; Et_2O, diethyl ether; Fmoc, 9-fluorenylmethoxycarbonyl; PyBOP, (benzotriazol-1-yloxy)-tris(pyrrolidino)phosphonium hexafluorophosphate; TFA, trifluoroacetic acid; TIS, triisopropylsilane; TNBS, 2,4,6-trinitrobenzenesulfonic acid.

Aldehyde 2: Compound **1**[23] (3.128 g, 9.16 mmol), $KHCO_3$ (1.377 g, 13.76 mmol, 1.5 equiv) and tetrabutylammonium iodide (0.3385 g, 0.916 mmol, 0.1 equiv) were dissolved in dry DMSO (18 mL) under argon. The resulting white suspension was stirred at room temperature for 10 min to obtain a clear solution. Benzyl bromide (3.25 mL, 4.67 g, 27.33 mmol, 2.99 equiv) was added to this solution and the colorless reaction mixture was stirred for 36 h at room temperature. The reaction was

quenched by the addition of water (100 mL) and the DMSO/water layer was extracted with EtOAc (3×150 mL). The combined organic layers were washed with saturated aq. $NaHCO_3$ (2×100 mL), saturated aq. $Na_2S_2O_3$ (1×100 mL), and finally with brine (1×100 mL). The organic layer was dried (Na_2SO_4) and concentrated by rotary evaporation. The resulting yellowish oil was triturated in cold (0 °C) light petroleum ether (b.p. 35—60 °C) until a white solid was obtained. The solid (3.128 g) was recovered by filtration. ^{1}H NMR and ES-MS analysis data for the crude solid were compatible with published data for the purified product[23] except for the presence of trace amounts of DMSO. The solid was subjected without further purification to Swern oxidation following the procedure reported by Rocchi et al.[23] Aldehyde **2** (1.782 g) was obtained after SiO_2 column chromatography (eluent: cyclohexane/EtOAc, 2:1, v/v). Yield: 45% over two steps (lit.:[23] 30% over two steps). ^{1}H NMR and ES-MS analysis data were identical to published data. $[\alpha]_D^{25}=+9.2$ ($c=1.13$ in $CHCl_3$) (lit.: $[\alpha]_D^{25}=+9.3$).[23]

Fmoc-Ada$_2$(*t*Bu)$_2$-OBn (3): Compound **2** (1.536 g, 3.58 mmol) and di-*tert*-butyl iminodiacetate (1.317 g, 5.37 mmol, 1.5 equiv) were dissolved in anhydrous 1,2-dichloroethane (15 mL). $NaBH(OAc)_3$ (1.366 g, 6.44 mmol, 1.8 equiv) was added to this solution, which was stirred overnight under argon. Then saturated aq. $NaHCO_3$ (30 mL) and dichloromethane (30 mL) were added and the organic phase was decanted. The aqueous phase was again extracted with dichloromethane (2×30 mL). The joint organic phases were dried (Na_2SO_4) and evaporated to yield a colorless oil, which was purified by SiO_2 column chromatography (eluent: CH_2Cl_2/AcOEt/NEt_3, 20:1:0.1, v/v/v) to give **3** as an oil (1.794 g, 77% yield). $[\alpha]_D^{20}=-8.4$ ($c=1.13$ in $CHCl_3$); ^{1}H NMR (400 MHz, $CDCl_3$, 25 °C): $\delta=$ 7.76 (d, ^3J(H,H) = 7.5 Hz, 2H; Ar, NH), 7.70 (d, ^3J(H,H) = 7.1 Hz, 2H; Ar, NH), 7.41–7.23 (m, 10H; Ar, NH), 5.20, 5.15 (AB system, $J_{AB}=$ 12.4 Hz, 2H; CH_2 (Bn)), 4.58 (m, 1H; Hα), 4.39 (m, 1H; CH_2 (Fmoc)), 4.23 (m, 1H; CH_2 (Fmoc)), 4.29 (m, 1H; C*H* (Fmoc)), 3.36, 3.27 (AB system, $J_{AB}=$17.5 Hz, 2H; CH_2COO*t*Bu), 2.86 (m, 1H; Hγ); 2.71 (m, 1H; Hγ), 2.08 (m, 1H; Hβ), 1.95 (m, 1H; Hβ), 1.46 ppm (s, 18H; *t*Bu); ^{13}C NMR (100 MHz, $CDCl_3$, 25 °C): $\delta=$172.4 (*C*OOBn), 170.9 (*C*OO*t*Bu), 156.9 (*C*O (Fmoc)), 144.5, 144.3, 141.5 (2C) (C_q (Fmoc)), 136.0 (C_q (Bn)), 128.7, 128.5, 128.4 (C_{Ar}-H (Bn)), 127.8, 127.3, 125.7, 120.1 (C_{Ar}-H (Fmoc)), 81.5 (C_q (*t*Bu)), 67.3, 67.2 (*C*H$_2$ (Fmoc) and *C*H$_2$ (Bn)), 56.7 (*C*H$_2$COO*t*Bu), 53.1 (*C*γ), 50.4 (*C*α), 47.4 (*C*H (Fmoc)), 28.9 (*C*β), 28.4 ppm (*t*Bu); ES-MS: *m*/*z* (%): 657.2 (100) [*M*+H$^+$].

Fmoc-Ada$_2$(*t*Bu)$_2$-OH: Compound **3** (1.75 g, 2.66 mmol) was dissolved in absolute ethanol (50 mL). This solution was hydrogenated overnight at room temperature and atmospheric pressure with 10% Pd/C catalyst (175 mg). The catalyst was filtered through Celite and the solvent was evaporated to obtain Fmoc-Ada$_2$(*t*Bu)$_2$-OH as a hygroscopic glassy solid (1.55 g, 99% yield). $[\alpha]_D^{20}=+13.9$ ($c=1.10$ in $CHCl_3$); ^{1}H NMR (400 MHz, $CDCl_3$, 25 °C): $\delta=$7.76 (d, ^3J(H,H) = 7.5 Hz, 2H; Ar), 7.62 (d, ^3J(H,H) = 7.1 Hz, 2H; Ar), 7.39 (dd (app. t), ^3J(H,H) ≈ 7.3 Hz, 2H; Ar), 7.31 (dd (app. t), ^3J(H,H) ≈ 7.3 Hz, 2H; Ar), 6.40 (d, ^3J(H,H) = 4.6 Hz, 1H; NH), 4.47 (m, 1H; Hα), 4.35 (m, 2H; CH_2 (Fmoc)), 4.22 (m, 1H; C*H* (Fmoc)), 3.45 (s, 4H; CH_2COO*t*Bu), 2.98 (m, 2H; Hγ), 2.02 (m, 2H; Hβ), 1.47 ppm (s, 18H; *t*Bu); ^{13}C NMR (100 MHz, $CDCl_3$, 25 °C): $\delta=$ 173.5 (COOH), 169.2 (*C*OO*t*Bu), 156.3 (*C*O (Fmoc)), 144.2, 141.5 (C_q (Fmoc)), 127.9, 127.3, 125.4, 120.2 (C_{Ar}-H (Fmoc)), 82.7 (C_q (*t*Bu)), 67.3 (*C*H$_2$ (Fmoc)), 55.3 (*C*H$_2$COO*t*Bu), 54.5(*C*γ), 52.7 (*C*α), 47.4 (*C*H (Fmoc)), 29.7 (*C*β), 28.3 ppm (*t*Bu); ES-MS: *m*/*z* (%): 569.08 (100) [*M*+H$^+$]; 591.2 (92) [*M*+Na$^+$]; elemental analysis calcd (%) for $C_{31}H_{40}N_2O_8\cdot{}^1/_2H_2O$: C 64.16, H 7.11, N 4.77; found: C 64.45, H 7.15, N 4.93.

Fmoc-Ada$_3$(*t*Bu)$_2$-OBn (5): Compound **4**[26] (1.593 g, 2.92 mmol) was dissolved in CH_2Cl_2 (40 mL). Trifluoroacetic acid (20 mL) was added dropwise to this stirred solution. After 1.5 h, TLC analysis showed the disappearance of **4**. The solvents were evaporated in vacuo. ES-MS analysis of the resulting crude oil showed the molecular peak belonging to Fmoc-Orn-OBn (*m*/*z*=445.3 [*M*+H$^+$]). This oil was dissolved in DMF (20 mL). *tert*-Butyl bromoacetate (1.3 mL, 2.27 g, 11.69 mmol, 4 equiv), $KHCO_3$ (5.85 g, 58.6 mmol, 20 equiv), and NBu_4I (1.08 g, 2.92 mmol, 1 equiv) were added. The resulting mixture was stirred for 7 h at 35 °C. Water (100 mL) and Et_2O (100 mL) were added to the reaction mixture. The aqueous phase was decanted and extracted with Et_2O (3×50 mL). The joint organic phases were washed with saturated $Na_2S_2O_3$ (50 mL) and water (50 mL), dried (Na_2SO_4), and the solvents were evaporated in vacuo. The resulting oil was purified by SiO_2 column chromatography (eluent: toluene/Et_2O, 4:1, v/v) to give **5** (1.047 g, 56% yield) as a colorless oil. $[\alpha]_D^{20}=+8.3$ ($c=1.00$ in $CHCl_3$); ^{1}H NMR (400 MHz, $CDCl_3$, 25 °C): $\delta=$7.76 (d, ^3J(H,H) = 7.4 Hz, 2H; Ar), 7.61 (d, ^3J(H,H) = 7.1 Hz, 2H; Ar), 7.41–7.27 (m, 9H; Ar), 5.85 (d, ^3J(H,H) = 7.4 Hz, 1H; NH), 5.18 (m, 2H; CH_2Bn), 4.38 (m, 3H; Hα and CH_2 (Fmoc)), 4.22 (dd (app. t), ^3J(H,H) ≈ 6.7 Hz, 1H; CH (Fmoc)), 3.36 (s, 4H; CH_2COO*t*Bu), 2.70 (m, 2H; Hδ), 1.98–1.78 (m, 2H; Hβ), 1.50 (m, 2H; Hγ), 1.44 ppm (s, 18H; *t*Bu); ^{13}C NMR (100 MHz, $CDCl_3$, 25 °C): $\delta=$172.6 (*C*OOBn), 170.1 (*C*OO*t*Bu), 156.4 (*C*O (Fmoc)), 144.2, 144.1, 141.5 (2C) (C_q (Fmoc)), 135.7 (C_q (Bn)), 128.8, 128.6, 128.5 (Ph), [127.9, 127.3, 125.4, 120.2 (C_{Ar}-H (Fmoc), 81.3 (C_q (*t*Bu)), 67.3, 67.2 (*C*H$_2$ (Fmoc) and *C*H$_2$ (Bn)), 56.1 (*C*H$_2$COO*t*Bu), 54.3 (*C*α), 53.7 (*C*δ), 47.4 (*C*H (Fmoc)), 30.0 (*C*β), 28.4 (*t*Bu), 24.1 ppm (*C*γ); ES-MS: *m*/*z* (%): 673.3 (100) [*M*+H$^+$].

Fmoc-Ada$_3$(*t*Bu)$_2$-OH: Compound **5** (0.963 g, 1.43 mmol) was hydrogenated following the same protocol as used for the debenzylation of **3**. Fmoc-Ada$_3$(*t*Bu)$_2$-OH was obtained as a hygroscopic glassy solid (0.833 g, 100% yield). $[\alpha]_D^{20}=-3.2$ ($c=1.00$ in $CHCl_3$); ^{1}H NMR (400 MHz, $CDCl_3$, 25 °C): $\delta=$7.77 (d, ^3J(H,H) = 7.5 Hz, 2H; Ar), 7.62 (d, ^3J(H,H) = 6.9 Hz, 2H; Ar), 7.42–7.38 (m, 2H; Ar), 7.34–7.23 (m, 2H; Ar), 5.89 (d, ^3J(H,H) = 6.1 Hz, 1H; NH), 4.55–4.32 (m, 3H; Hα and CH_2 (Fmoc)), 4.24–4.20 (m, 1H; C*H* (Fmoc)), 3.58–3.44 (m, 4H; CH_2COO*t*Bu), 2.80 (m, 2H; Hδ), 2.01–1.77 (m, 2H; Hβ), 1.56–1.49 (m, 2H; Hγ), 1.45 ppm (s, 18H; *t*Bu); ^{13}C NMR (100 MHz, $CDCl_3$, 25 °C): $\delta=$174.4 (*C*OOH), 169.6 (*C*OO*t*Bu), 156.4 (*C*O (Fmoc)), 144.2, 144.1, 141.5 (2) (C_q (Fmoc)], 127.9, 127.3, 125.4, 120.2 (C_{Ar}-H (Fmoc)), 82.2 (C_q (*t*Bu)), 67.1 (*C*H$_2$ (Fmoc), 54.9 (*C*H$_2$COO*t*Bu), 53.9, 53.8 (*C*α and *C*δ), 47.4 (*C*H (Fmoc)), 30.4 (*C*β), 28.3 (*t*Bu), 22.4 ppm (*C*γ); ES-MS: *m*/*z* (%): 583.3 (100) [*M*+H$^+$]; elemental analysis calcd (%) for $C_{32}H_{42}N_2O_8\cdot H_2O$: C 63.98, H 7.38, N 4.66; found: C 63.94, H 7.37, N 4.64.

Peptide synthesis and purification: Both peptides were assembled manually by solid-phase peptide synthesis on a Rink Amide MBHA resin (substitution 0.57 mmol g^{-1}, 200 mg) by using Fmoc chemistry. The synthesis was started by an initial deprotection of the commercial resin-bound Fmoc with DMF/piperidine (4:1, v/v). Couplings were performed with *N*α-Fmoc-protected amino acids (2 equiv), PyBOP (2 equiv), and DIEA (6 equiv) in DMF for 30 min. In the case of Fmoc-Ada$_n$(*t*Bu)$_2$-OH the coupling reaction was monitored by using the TNBS test.[52] For incomplete reactions, a second coupling with Fmoc-Ada$_n$(*t*Bu)$_2$-OH (0.5 equiv), PyBOP (1 equiv), and DIEA (4 equiv) was performed. After each coupling, the resin was treated with DMF/pyridine/Ac_2O (7:2:1, v/v/v) to acetylate unreacted amino groups (2×2 min). Fmoc deprotection was achieved with DMF/piperidine (4:1, v/v) (3×3 min). The yield of each peptide coupling reaction was determined by UV/Vis spectroscopy ($\varepsilon_{300}=7800$ L mol^{-1} cm^{-1} for the piperidine adduct of dibenzofulvene). After the final Fmoc deprotection, the peptide was acetylated as described above. The peptide was cleaved from the resin and the side-chain protections were removed by treatment with a cleavage cocktail consisting of DTT (200 mg) dissolved in TFA/TIS/H_2O (20 mL, 92:4:4, v/v/v). After stirring for 2.5 h, the solution was evaporated to yield a yellow oil, which was triturated several times in Et_2O to yield a white powder. The solid residue was dissolved in water/acetonitrile (9:1, v/v) and purified by reversed-phase high-performance liquid chromatography (RP-HPLC, Merck Purospher, 250×40 mm, 10 μm C18 particles, solvent A = H_2O/TFA (99.925:0.075, v/v), solvent B = CH_3CN/H_2O/TFA (90:10:0.1, v/v/v), elution gradient from 10% A/90% B to 40% A/60% B in 15 min, flow rate 75 mL min^{-1}, to yield the desired peptides as white powders. The purity was checked by analytical RP-HPLC (Merck Purospher STAR endcapped, 4.6×250 mm, 5 μm C18 particles, solvent A = H_2O/TFA (99.925:0.075, v/v), solvent B = CH_3CN/H_2O/TFA (90:10:0.1, v/v/v, elution gradient from 10% A/90% B to 40% A/60% B in 15 min, flow rate 1 mL min^{-1}, UV monitoring at 280 nm, see Figure S3).

Ac-WAda$_2$PGAda$_2$G-NH$_2$ (P^2): Yield of the on-resin synthesis (UV): 92%. Isolated mass: 58.5 mg (isolated yield assuming that the solid is **P^2**·2TFA: 48%). (+)ES-MS: *m*/*z*: 889.3 [*M*+H$^+$], 445.3 [*M*+H$_2^{2+}$];

(−)ES-MS: m/z: 887.3 $[M-H^-]$, 443.2 $[M-2H^{2-}]$; RP-HPLC: t_r= 10.8 min, 97% purity.

Ac-WAda$_3$PGAda$_3$G-NH$_2$ (P^3:): Yield of the on-resin synthesis (UV): 77%. Isolated mass: 43.5 mg (isolated yield assuming that the solid is P^3·2TFA: 35%). (+)ES-MS: m/z: 917.4 $[M+H^+]$, 459.4 $[M+H_2^{2+}]$; (−)ES-MS: m/z: 915.5 $[M-H^-]$, 457.3 $[M-2H^{2-}]$; RP-HPLC: t_r= 10.6 min, 97% purity.

Preparation of aqueous solutions: 5 mM metal solutions, used as stock solutions in the luminescence, CD, and ES-MS experiments, were prepared from the corresponding chloride salts ($LaCl_3$·$7H_2O$, $EuCl_3$·$6H_2O$, and $TbCl_3$·$6H_2O$) in pure H_2O. Their precise concentration was obtained by titration with a 5 mM volumetric ethylenediaminetetraacetic acid (Fisher Chemicals) in the presence of a colorimetric indicator. For NMR analysis in D_2O, a solution of anhydrous $La(OTf)_3$ in pure D_2O was prepared and titrated similarly. Peptide solutions were prepared freshly before use and the precise peptide concentration was determined by UV analysis (ε_{280}=5690 L mol^{-1} cm^{-1} owing to the presence of the Trp residue). A 5 mM NTA solution to be used in competition experiments was prepared in pure water from solid nitriloacetic acid (Riedel-de-Haën) and its precise concentration was determined pH-metrically. HEPES buffer was prepared by dissolving solid 4-(2-hydroxyethyl)-piperazine-1-ethanesulfonic acid (Fluka) in H_2O (or D_2O) and by adjusting the pH (or pD) to 7.0 with KOH (or NaOD).

Circular dichroism: CD spectra were recorded at 25°C on a Applied Photophysics Chirascan spectrometer in a cell with a path length of 1 cm. The peptide concentration was ~20 μM in water and the pH was adjusted with KOH. All the spectra were obtained from 320 to 190 nm with a 1 nm interval, a time constant of 2 s, a bandwidth of 1 nm, and three scans. The CD spectra are reported in molar ellipticity per α-amino acid residue ($[\Theta]$ in units of deg cm^2 mol^{-1}; $[\Theta]=\theta_{obs}/(10lcn)$, with θ_{obs} the observed ellipticity in m°, l the optical path length of the cell in cm, c the peptide concentration in mol L^{-1}, and n the number of residues in the peptide (n=6 in the present case)).

Luminescence: Luminescence spectra were recorded on a LS50B spectrofluorimeter connected to a computer equipped with FLWINLAB 2.0. The measurements were performed at 298 K. Trp fluorescence titrations were performed with 280 nm excitation (excitation slit: 3.0 nm). The emission slit was adjusted (3.5–4.5 nm) to avoid signal saturation. Tb phosphorescence spectra were recorded upon Trp excitation (280 nm) after a 0.05 ms delay and with a 0.5 ms gate time. The excitation and emission slits were 10.0 and 15.0 nm, respectively. A 430 nm cut-off filter was used. Conditional stability constants were extracted from the spectral data by using SPECFIT.[53] Experiments were performed in triplicate to ensure reproducibility. The reported conditional stability constants are averages of the three experimental values. Lifetime measurements were performed on peptide samples containing 0.5 equiv $TbCl_3$ to ensure exclusive contribution from the mononuclear complexes. The emission intensities of the most intense Tb^{3+} emission band were recorded after excitation at 280 nm with a first delay of 0.05 ms, a delay increment of 0.05 ms, and the number of measurements adjusted to have a final delay of $>4\tau$.

Mass spectrometry of the Eu^{3+} complexes: Eu^{3+} was chosen as a representative Ln^{3+} ion because of its characteristic isotopic signature (^{151}Eu 47.8%, ^{153}Eu 52.2%). 60 μM peptide solutions were prepared in 20 mM ammonium acetate buffer (pH 7). The 5 mM $EuCl_3$ stock solution was added to prepare aliquots containing 0, 0.5, 1, and 2 equiv of $EuCl_3$ per peptide. For competition between P^2 and P^3, a solution containing both peptides (30 μM each) was prepared by mixing equal volumes of the original peptide solutions and 1 equiv $EuCl_3$ was added. Mass spectra were recorded on an LXQ-type THERMO SCIENTIFIC spectrometer equipped with an electrospray ionization source and a linear trap detector. Solutions were injected into the spectrometer at a flow rate of 5 μL min^{-1}. The ionization voltage and capillary temperature were about 2 kV and 250°C, respectively.

Peptide NMR spectroscopy: NMR experiments for apopeptide and complex characterization were recorded on a 500 MHz Bruker Avance spectrometer equipped with a BBI probe with a triple-axis gradient field. ^{1}H NMR spectra were recorded with 12 ppm windows and 32k data points in the time domain. 2D ^{1}H NMR spectra were recorded at various temperatures in H_2O/D_2O (9:1, v/v) using WATERGATE or presaturation solvent suppression or in D_2O with presaturation suppression of residual HOD. Spectra were acquired in phase-sensitive mode with TPPI for quadrature detection in the indirect dimension using 2048×512 matrices over a 5000 Hz spectral width. TOCSY experiments were performed by using a MLEV-17 spin-lock sequence with a mixing time of 70 ms. ROESY and NOESY/EXSY experiments were recorded with a mixing time of 300 ms (3300 Hz spin lock for ROESY). 2D NOESY NMR spectra for structure determination were recorded on a Varian Vnmrs 800 MHz spectrometer equipped with a ^{1}H/^{2}H/^{15}N/^{13}C cryogenic probe. A mixing time of 250 ms was used.

NMR structure refinement: NMR solution structures were obtained with CNSsolve[47] (version 1.1) following standard refinement protocols and using the "protein-allhdg" forcefield for natural amino acids. For unnatural amino acid side-chains and the lanthanum coordination sphere custom topology and parameter files were generated. The parameters were chosen as follows. For Ada_2 side-chains, the parameters for Cα, Cβ, Cγ, and bound hydrogen atoms were set identical to those of Cα, Cβ, and Cε of L-lysine. Parameters for the bond lengths of the Nδ, Cε, and Cζ atoms were adapted from glycine parameters. Parameters for the La–N and La–O distances, as well as the Cγ–Nδ–Cε, Cζ–Oη1–La, and Nδ–Cε–Cζ angles, and the Cε–Cζ–Oη1–La torsion angle were obtained from high-resolution X-ray data of La^{3+} complexes containing the *N*-alkylaminodiacetate moiety referenced in the Cambridge Structural Database (CSD). The structure search and visualization were performed with CSD ConQuest 1.10.[54] Ten relevant structures were found in the database and the average structural parameters were extracted with CSD Vista 2.1. CSD references: ASEMUG, ASEMUG01, GEQFOX, HETALA, HETALA01, KIBZUR, SOHNOS, TISQOB, XALSOS, ZAMHEA. Average parameters (standard deviation) (units: Å,°): La–N 2.830 (0.038), La–O 2.522 (0.042),C–*N*–C 110.52 (1.47), C–O–La 126.68 (2.08), N–C–C 112.37 (2.06), C–C–O–La 1.5 (25) (was set to 0). Similarly, Cζ–Oη1 and Cζ–Oη2 (distances between metal bound and metal unbound oxygen atoms in the Ada_2 side-chain, respectively) were adapted from the three published structures containing monodentate and not bridging La–carboxy moieties. CSD references: TISQOB, XALSOS, ZAMHEA. Average parameters (standard deviation) (units: Å,°): Cζ–Oη1 1.26 (0.09), Cζ–Oη2 1.245 (0.01). The La^{3+} nonbonded radius was determined from crystallographic data,[55] as for the other ions already implemented in CNSsolve. Coordinated water molecules were not included explicitly in the model. However, the ionic radius of La^{3+} for a coordination number of 9 was used.

As spin diffusion generated some artifacts in the NOESY spectrum (the presence of antiphase components in the NOESY spectra reported in Figures S9 and S10), a tROESY spectrum was recorded to determine whether some signals were artifactual in nature.[46] Some Trp(indole)-Pro correlations were indeed shown to be absent and thus the corresponding restraints were removed from the calculations. Upper and lower limits for distance constraints were set to ±15% of the H–H distances obtained by integration of the 2D NOESY spectra (250 ms). r^{-6} averaging was chosen for the NOE restraints. Geminal Pro Hδ1/Hδ2, $Ada_2$2 Hβ1/Hβ2, $Ada_2$5 Hβ1/Hβ2, and Gly4 Hα1/Hα2 distances (taken as 1.8 Å) as well as Pro Hα/Hβ1 (2.4 Å) were used as references for distance calibration. Four ^3J coupling constants (Gly4 $^3J_{NH,H\alpha}$ and Trp1 $^3J_{H\alpha,H\beta}$) measured in the ^{1}H NMR spectra were included as well as restraints with standard CNSsolve Karplus parameters (Gly) or published Karplus parameters for $^3J_{H\alpha,H\beta}$.[56] Pseudo-atom corrections were applied to methyl and overlapping or nonstereospecifically assigned methylenes.[57] Dynamics experiments were performed with a hot phase at 2000 K with 5000 0.003 ps steps followed by a slow cooling phase with 5000 0.005 ps steps with 5 K cooling per step. Final minimizations were performed with the Powell algorithm (200 steps, 100 cycles). An ensemble of 50 structures was generated. None of the structures displayed NOE violations greater than 0.4 Å. The 10 lowest-energy structures were visualized and aligned (backbone atoms) by using PyMol v. 0.99 (DeLano Scientific LLC).[58]

Acknowledgements

We thank Cindy Carroux for participation in this study as an undergraduate trainee, Dr. Olivier Sénèque for fruitful discussions and Pierre-Alain Bayle and Adrien Favier for their help in using the CGRM and IBS NMR facilities, respectively. Financial support from the TGE RMN THC for providing access to the 800 MHz NMR spectrometer is gratefully acknowledged. This work is a contribution to the EC COST Action D-38 and European EMIL network.

[1] E. Pidcock, G. R. Moore, *J. Biol. Inorg. Chem.* **2001**, *6*, 479–489.
[2] P. Caravan, J. J. Ellison, T. J. McMurry, R. B. Lauffer, *Chem. Rev.* **1999**, *99*, 2293–2352.
[3] a) A. E. Merbach, E. Toth, *The Chemistry of Contrast Agents*, Wiley, New York, **2001**; b) S. Aime, M. Botta, E. Terreno, *Adv. Inorg. Chem.* **2005**, *57*, 173–237; c) P. Caravan, *Chem. Soc. Rev.* **2006**, *35*, 512–523.
[4] a) C. Piguet, C. F. G. C. Geraldes in *Handbook on the Physics and Chemistry of Rare Earths* (Eds.: K. A. J. Gschneidner, J.-C. G. Bünzli, V. K. Pecharsky), Elsevier, **2003**, pp. 353–463; b) L. Di Bari, P. Salvadori, *Coord. Chem. rev.* **2005**, *249*, 2854–2879.
[5] G. Otting, *J. Biomol. NMR* **2008**, *42*, 1–9.
[6] a) J.-C. Bünzli, C. Piguet, *Chem. Soc. Rev.* **2005**, *34*, 1048–1077; b) J.-C. G. Bünzli, *Acc. Chem. Res.* **2006**, *39*, 53–61; c) S. Pandya, J. Yu, D. Parker, *Dalton Trans.* **2006**, 2757–2766.
[7] a) J. P. MacManus, C. W. Hogue, B. J. Marsden, M. Sikorska, A. G. Szabo, *J. Biol. Chem.* **1990**, *265*, 10358–10366; b) C. W. Hogue, J. P. MacManus, D. Banville, A. G. Szabo, *J. Biol. Chem.* **1992**, *267*, 13340–13347.
[8] a) R. T. Kovacic, J. T. Welch, S. J. Franklin, *J. Am. Chem. Soc.* **2003**, *125*, 6656–6662; b) P. Caravan, J. M. Greenwood, J. T. Welch, S. J. Franklin, *Chem. Commun.* **2003**, 2574–2575.
[9] a) M. Nitz, K. J. Franz, R. L. Maglathlin, B. Imperiali, *ChemBioChem* **2003**, *4*, 272–276; b) K. J. Franz, M. Nitz, B. Imperiali, *ChemBioChem* **2003**, *4*, 265–271.
[10] M. Nitz, M. Sherawat, K. J. Franz, E. Peisach, K. N. Allen, B. Imperiali, *Angew. Chem.* **2004**, *116*, 3768–3771; *Angew. Chem. Int. Ed.* **2004**, *43*, 3682–3685.
[11] C. S. Bonnet, P. H. Fries, S. Crouzy, O. Sénèque, F. Cisnetti, D. Boturyn, P. Dumy, P. Delangle, *Chem. Eur. J.* **2009**, DOI: 10.1002/chem.200900636.
[12] a) I. D. Clark, I. Hill, M. Sikorska-Walker, J. P. MacManus, A. G. Szabo, *FEBS Lett.* **1993**, *333*, 96–98; b) A. M. Reynolds, B. R. Sculimbrene, B. Imperiali, *Bioconjugate Chem.* **2008**, *19*, 588–591; c) C. S. Bonnet, M. Devocelle, T. Gunnlaugsson, *Chem. Commun.* **2008**, 4552–4554.
[13] R. P. Cheng, S. L. Fisher, B. Imperiali, *J. Am. Chem. Soc.* **1996**, *118*, 11349–11356.
[14] a) M. D. Shults, D. A. Pearce, B. Imperiali, *J. Am. Chem. Soc.* **2003**, *125*, 10591–10597; b) H. Ishida, M. Kyakuno, S. Oishi, *Biopolymers* **2004**, *76*, 69–82.
[15] a) M. R. Ghadiri, C. Soares, C. Choi, *J. Am. Chem. Soc.* **1992**, *114*, 825–831; b) M. R. Ghadiri, M. A. Case, *Angew. Chem.* **1993**, *105*, 1663–1670; *Angew. Chem. Int. Ed. Engl.* **1993**, *32*, 1594–1597; c) A. J. Doerr, G. L. McLendon, *Inorg. Chem.* **2004**, *43*, 7916–1925.
[16] a) W. D. Kohn, C. M. Kay, B. D. Sikes, R. S. Hodges, *J. Am. Chem. Soc.* **1998**, *120*, 1124–1132; b) A. Kashiwada, K. Ishida, K. Matsuda, *Bull. Chem. Soc. Jpn.* **2007**, *80*, 2203–2207.
[17] F. Ruan, Y. Chen, K. Itoh, T. Sasaki, P. B. Hopkins, *J. Org. Chem.* **1991**, *56*, 4347–4354.
[18] W. M. Kazmierski, *Int. J. Pept. Protein Res.* **1995**, *445*, 241–247.
[19] S. Hutschenreiter, L. Neumann, U. Radler, L. Schmitt, R. Tampe, *ChemBioChem* **2003**, *4*, 1340–1344.
[20] F. Q. Ruan, Y. Q. Chen, P. B. Hopkins, *J. Am. Chem. Soc.* **1990**, *112*, 9403–9404.
[21] R. H. Holm, P. Kennepohl, E. I. Solomon, *Chem. Rev.* **1996**, *96*, 2239–2314.
[22] J. A. Smith, L. G. Pease, *Crit. Rev. Biochem.* **1980**, *8*, 315–399.
[23] F. Filira, B. Biondi, L. Biondi, E. Giannini, M. Gobbo, L. Negri, R. Rocchi, *Org. Biomol. Chem.* **2003**, *1*, 3059–3063.
[24] Y. Huang, S. Dey, X. Zhang, F. Sönnichsen, P. Garner, *J. Am. Chem. Soc.* **2004**, *126*, 4626–4640.
[25] A. F. Abdel-Magid, S. J. Mehrman, *Org. Process Res. Dev.* **2006**, *10*, 971–1031.
[26] O. V. Larionov, A. de Meijere, *Org. Lett.* **2004**, *6*, 2153–2156.
[27] a) F. J. Blanco, G. Rivas, L. Serrano, *Nat. Struct. Biol.* **1994**, *1*, 584–590; b) J. Venkatraman, S. C. Shankaramma, P. Balaram, *Chem. Rev.* **2001**, *101*, 3131–3152; c) R. M. Hughes, M. L. Waters, *Curr. Opin. Struct. Biol.* **2006**, *16*, 514–524.
[28] A. M. C. Marcelino, L. M. Gierasch, *Biopolymers* **2008**, *89*, 380–391.
[29] S. R. Raghothama, S. K. Awasthi, P. Balaram, *J. Chem. Soc. Perkin Trans. 2* **1998**, 137–143.
[30] A. Borics, R. F. Murphy, S. Lovas, *J. Biomol. Struct. Dyn.* **2004**, *22*, 761–770.
[31] B. P. Joshi, K.-H. Lee, *Bioorg. Med. Chem.* **2008**, *16*, 8501–8509.
[32] W. C. Chan, P. D. White, *Fmoc Solid Phase Peptide Synthesis—A Practical Approach*, OUP, Oxford, **2000**.
[33] K. Wüthrich, *NMR of Proteins and Nucleic Acids*, Wiley, New York, **1986**.
[34] R. M. Smith, A. E. Martell, R. J. Motekaitis, NIST Critically Selected Stability Constants of Metal Complexes Database, NIST Standard Reference Database 46, **2001**.
[35] V. B. Di Marco, G. G. Bombi, *Mass. Spectrom. Rev.* **2006**, *25*, 347–379.
[36] N. Sreerama, R. W. Woody in *Circular Dichroism, Principles and Applications*, 2nd ed. (Eds.: N. Berova, K. Nakanishi, R. W. Woody), Wiley, New York, **2000**, pp. 601–620.
[37] A. Perczel, M. Hollósi in *CD and the Conformational Analysis of Biomolecules* (Ed.: G. D. Fasman), Plenum Press, New York, **1996**, pp. 285–380.
[38] R. W. Woody, A. K. Dunker in *CD and the Conformational Analysis of Biomolecules* (Ed.: G. D. Fasman), Plenum Press, New York, **1996**, pp. 109–157.
[39] P. D. Adams, Y. Chen, K. Ma, M. G. Zagorsky, F. D. Sönnichsen, M. L. McLaughlin, M. D. Barkley, *J. Am. Chem. Soc.* **2002**, *124*, 9278–9286.
[40] a) W. De Horrocks, W. E. Collier, *J. Am. Chem. Soc.* **1981**, *103*, 2856–2862; b) P. J. Breen, E. K. Hild, W. DeW. Horrocks, *Biochemistry* **1985**, *24*, 4991–4997.
[41] W. De Horrocks, D. R. Sudnick, *Acc. Chem. Res.* **1981**, *14*, 384–392.
[42] A. Beeby, I. M. Clarkson, R. S. Dickins, S. Faulkner, D. Parker, L. Royle, A. S. de Sousa, J. A. G. Williams, M. Woods, *J. Chem. Soc. Faraday Trans. 2* **1999**, 493–503.
[43] W. De Horrocks, D. R. Sudnick, *J. Am. Chem. Soc.* **1979**, *101*, 334–340.
[44] a) N. Ouali, J.-P. Riviera, D. Chapon, P. Delangle, C. Piguet, *Inorg. Chem.* **2004**, *43*, 1517–1529; b) L. Di Bari, M. Lelli, G. Pintacuda, G. Pescitelli, F. Marchetti, P. Salvadori, *J. Am. Chem. Soc.* **2003**, *125*, 5549–5558.
[45] M. Heitzmann, F. Bravard, C. Gateau, N. Boubals, C. Berthon, J. Pecaut, M. C. Charbonnel, P. Delangle, *Inorg. Chem.* **2009**, *48*, 246–256.
[46] D. Neuhaus, *Nuclear Overhauser Effect in Structure & Conformational Analysis of Biomolecules*, Wiley, New York, **2000**.
[47] a) A. T. Brunger, *Nat. Protoc.* **2007**, *2*, 2728–2733; b) A. T. Brünger, P. D. Adams, G. M. Clorec, W. L. DeLano, P. Grose, R. W. Grosse-Kunstleve, J.-S. Jiang, J. Kuszewski, M. Nilges, N. S. Pannu, R. J. Read, L. M. Rice, T. Simonson, G. L. Warren, *Acta Crystallogr. Sect. D* **1998**, *54*, 905–921.
[48] J. T. Welch, W. R. Kearney, S. J. Franklin, *Proc. Natl. Acad. Sci. USA* **2003**, *100*, 3725–3730.
[49] R. Bhattacharyya, P. Chakrabarti, *J. Mol. Biol.* **2003**, *331*, 925–940.
[50] a) T. Yamamura, T. Watanabe, A. Kikuchi, T. Yamane, M. Ushiyama, H. Hirota, *Inorg. Chem.* **1997**, *36*, 4849–4859; b) O. Sénèque, S. Crouzy, D. Boturyn, P. Dumy, M. Ferrand, P. Delangle, *Chem. Commun.* **2004**, 770–771; c) P. Rousselot-Pailley, O. Seneque, C.

Lebrun, S. Crouzy, D. Boturyn, P. Dumy, M. Ferrand, P. Delangle, *Inorg. Chem.* **2006**, *45*, 5510–5520.

[51] a) H. N. Hoang, G. K. Bryant, M. J. Kelso, R. L. Beyer, T. G. Appleton, D. P. Fairlie, *Inorg. Chem.* **2008**, *47*, 9439–9449; b) R. L. Beyer, H. N. Hoang, T. G. Appleton, D. P. Fairlie, *J. Am. Chem. Soc.* **2004**, *126*, 15096–15105.

[52] W. S. Hancock, J. E. Battersby, *Anal. Biochem.* **1976**, *71*, 260–264.

[53] a) H. Gampp, M. Maeder, C. J. Meyer, A. D. Zuberbühler, *Talanta* **1985**, *32*, 95–101; b) H. Gampp, M. Maeder, C. J. Meyer, A. D. Zuberbühler, *Talanta* **1985**, *32*, 257–264; c) H. Gampp, M. Maeder, C. J. Meyer, A. D. Zuberbühler, *Talanta* **1985**, *32*, 1133–1139; d) H. Gampp, M. Maeder, C. J. Meyer, A. D. Zuberbühler, *Talanta* **1986**, *33*, 943–951.

[54] I. J. Bruno, J. C. Cole, P. R. Edgington, M. Kessler, C. F. Macrae, P. McCabe, J. Pearson, R. Taylor, *Acta Crystallogr. Sect. B* **2002**, *58*, 389–397.

[55] R. D. Shannon, *Acta Crystallogr. Sect. A* **1976**, *32*, 751–767.

[56] C. Pérez, F. Löhr, H. Rüterjans, J. M. Schmidt, *J. Am. Chem. Soc.* **2001**, *123*, 7081–7093.

[57] C. M. Fletcher, D. N. M. Jones, R. Diamond, D. Neuhaus, *J. Biomol. NMR* **1996**, *8*, 292–310.

[58] W. L. Delano, The PyMOL Molecular Graphics System, Delano Scientific, Palo Alto, USA, **2002**, http://www.pymol.org/

Received: March 23, 2009
Published online: June 27, 2009

